Journal of Alzheimer's Disease 39 (2014) 385–400
DOI 10.3233/JAD-131535
IOS Press

Glutaminyl Cyclase in Human Cortex: Correlation with (pGlu)-Amyloid-β Load and Cognitive Decline in Alzheimer's Disease

Markus Morawski[a,1], Stephan Schilling[b,1], Moritz Kreuzberger[a,1], Alexander Waniek[a], Carsten Jäger[a], Birgit Koch[b], Holger Cynis[b,c], Astrid Kehlen[b], Thomas Arendt[a], Maike Hartlage-Rübsamen[a], Hans-Ulrich Demuth[b,*] and Steffen Roßner[a,*]
[a]*Paul Flechsig Institute for Brain Research, University of Leipzig, Leipzig, Germany*
[b]*Probiodrug AG, Halle/S., Germany*
[c]*Center for Neurologic Disease, Brigham and Women's Hospital, Harvard Medical School, Boston, MA, USA*

Handling Associate Editor: Stefan Lichtenthaler

Accepted 17 September 2013

Abstract. Brains of Alzheimer's disease (AD) patients are characterized in part by the formation of high molecular weight aggregates of amyloid-β (Aβ) peptides, which interfere with neuronal function and provoke neuronal cell death. The pyroglutamate (pGlu) modification of Aβ was demonstrated to be catalyzed by the enzyme glutaminyl cyclase (QC) and to enhance pathogenicity and neurotoxicity. Here, we addressed the role of QC in AD pathogenesis in human cortex. Two sets of human *postmortem* brain tissue from a total of 13 non-demented controls and 11 AD cases were analyzed by immunohistochemistry and unbiased stereology, quantitative RT-PCR, and enzymatic activity assays for the expression level of QC in temporal and entorhinal cortex. Additionally, cortical Aβ and pGlu-Aβ concentrations were quantified by ELISA. Data on QC expression and Aβ peptide concentrations were correlated with each other and with the Mini-Mental State Examination (MMSE) of individual cases. In control cases, QC expression was higher in the more vulnerable entorhinal cortex than in temporal cortex. In AD brains, QC mRNA expression and the immunoreactivity of QC were increased in both cortical regions and frequently associated with pGlu-Aβ deposits. The analyses of individual cases revealed significant correlations between QC mRNA levels and the concentration of insoluble pGlu-Aβ aggregates, but not of unmodified Aβ peptides. Elevated pGlu-Aβ load showed a better correlation with the decline in MMSE than elevated concentration of unmodified Aβ. Our observations provide evidence for an involvement of QC in AD pathogenesis and cognitive decline by QC-catalyzed pGlu-Aβ formation.

Keywords: Alzheimer's disease, entorhinal cortex, glutaminyl cyclase, pyroglutamate-Aβ, Mini-Mental State Examination

INTRODUCTION

At early stages of Alzheimer's disease (AD), patients display mild disturbances in spatial and temporal orientation and in short-term memory. The relation between the actual clinical status of the patient and the degree of neuropathology can be assessed by testing cognitive function and by imaging techniques monitoring hippocampal shrinkage, Aβ deposition, and microglial activation [1–3]. However, the definite diagnosis of AD is only possible in *postmortem* brain

[1]These authors contributed equally to this manuscript.

*Correspondence to: Steffen Roßner, PhD, Paul Flechsig Institute for Brain Research, Jahnallee 59, 04109 Leipzig, Germany. Tel.: +49 341 9725758; Fax: +49 341 9725749; E-mail: steffen.rossner@medizin.uni-leipzig.de; Hans-Ulrich Demuth, Fraunhofer Institute of Cell Therapy and Immunology (IZI), Leipzig c/o, Department of Drug Design and Target Validation (MWT), Halle Biocenter, Weinbergweg, 22 06120 Halle (Saale), Germany. Tel.: +49 345 13142800; Fax: +49 345 13142801; E-mail: hans-ulrich.demuth@izi.fraunhofer.de.

ISSN 1387-2877/14/$27.50

tissue by the detection of neurofibrillary tangles and Aβ deposits in cortical brain tissue [4–6].

Aβ peptides are generated by proteolytic processing of the amyloid-β protein precursor (AβPP) by β- and γ-secretases [7]. A substantial proportion of Aβ peptides undergoes N-terminal truncation and subsequent cyclization of N-terminal glutamate (Glu) into pyroglutamate (pGlu), resulting in pGlu-Aβ peptides [8–11]. Such pGlu-Aβ peptides are major constituents of Aβ deposits in sporadic and familial AD [8, 12–14] and, based on a number of observations, could play a prominent role in AD pathogenesis. For example, the pGlu modification results in accelerated aggregation [15, 16] and in co-aggregation of non-modified Aβ peptides [17–20]. Furthermore, the pGlu residue confers resistance to degradation by most aminopeptidases as well as Aβ-degrading endopeptidases [21]. Finally, a strong neurotoxic effect of pGlu-Aβ peptides on primary neurons, neuronal cell lines, and neurons of AβPP transgenic animals *in vivo* has been described [16, 22, 23] and was demonstrated to be transmitted in a prion-like manner [24]. Interestingly, pGlu-modified Aβ peptides in brains of AD patients and transgenic mouse models were reported to be closely associated with [^{11}C]Pittsburgh Compound-B (PIB) autoradiographic signals [25].

The pGlu-Aβ peptide modification has been demonstrated to be catalyzed by glutaminyl cyclase (QC) *in vitro* [26] and *in vivo* [27–30]. In mammalian brain, physiologically relevant neuronal QC expression has been described in the hypothalamus and was shown to be involved in neuropeptide and hormone maturation [31–34]. Recently, we observed robust QC expression in mouse and human brain in AD-vulnerable subcortical regions, such as nucleus basalis Meynert, locus coeruleus, and Edinger-Westphal nucleus [35]. Moreover, we demonstrated pronounced QC immunoreactivity in a subpopulation of neocortical neurons and of GABAergic interneurons in the mouse hippocampus [36]. In the hippocampal formation of AD patients, distinct types of pGlu-Aβ deposits were identified at sites of QC immunoreactive neurons and in target fields of QC-rich projection neurons [37]. Chronic pharmacological inhibition [29] or genetic ablation [38, 39] of QC in transgenic mouse and *Drosophila* models of AD resulted in reduced pGlu-Aβ peptide generation and improved performance in cognitive tasks, while QC overexpression aggravated neuropathology and cognitive dysfunction in transgenic mice [39].

Thus, there is accumulating evidence from biochemical and histological analyses in experimental animals for a critical role of QC in pGlu-Aβ formation. Such pGlu-Aβ peptides provoke protein aggregation and deposition, neurodegeneration, gliosis, and impairment of learning and memory in transgenic mouse models. However, in human cortex, QC expression and its relation to pGlu-Aβ formation have not yet been thoroughly analyzed. Moreover, no information is available on the relation between QC expression, pGlu-Aβ formation, and the cognitive status of elderly humans. Here, we report a remarkably high expression of QC by neurons in temporal and entorhinal cortex of non-demented human subjects and an increase in QC immunoreactivity in both cortical areas in AD. Additionally, and for the first time, we provide evidence for a role of QC in the generation of pGlu-Aβ in human cortex and for a relation between QC expression, pGlu-Aβ formation, and cognitive decline in AD.

MATERIALS AND METHODS

Human brain tissue

Case recruitment and characterization of human brain tissue

Case recruitment and autopsy were performed in accordance with guidelines effective at the Banner Sun Health Research Institute Brain Donation Program of Sun City, Arizona [40]. The required consent was obtained for all cases. The definite diagnosis of AD for all cases used in this study was based on the presence of neurofibrillary tangles and neuritic plaques in the hippocampal formation and neocortical areas and met the criteria of the National Institute on Aging (NIA) and the Consortium to establish a registry for AD (CERAD) [5]. Brain tissue of temporal cortex (Area 22) and entorhinal cortex (Area 28) from 6 controls and 6 age-matched AD cases was used for QC and pGlu-Aβ immunohistochemistry. Additionally, for biochemical analyses, temporal cortex (Area 22) of 7 control cases and 5 AD cases with a very short *postmortem* interval of 1.5 to 5.5 hours and a thorough clinical characterization was used (Table 1). The cases enrolled in this study were matched for age, gender, and APOE genotype. Anatomical structures and cortical layers were identified using consecutive Nissl-stained sections and the *Atlas of the Human Brain* [41].

Tissue preparation

For immunohistochemistry, fifteen-mm-thick tissue blocks were prepared in the frontal plane according to the *Atlas of the Human Brain* [41] and fixed in 4%

Table 1
Human brain tissue used for biochemistry and correlation analyses

	Case #	PMD (h)	Gender	Age (y)	Brain weight (g)	APOE ε allele	Cause of Death	Braak score	MMSE (last score)	Gap MMSE/ Death (months)	CERAD Neuritic Plaque Score	CERAD Criteria	NIA Criteria (likelihood of dementia)
Control	Co1	2.5	Female	86	1145	3/3	pulmonary fibrosis	III	27/30	12	0	not met	not met
	Co2	2.5	Female	87	1120	3/3	pneumonia/cancer	IV	30/30	28	0	not met	not met
	Co3	2.75	Female	75	1110	3/4	pulmonary embolus	III	29/30	12	0	not met	not met
	Co4	3.0	Male	82	1240	3/3	renal failure/COPD	III	26/30	12	A	not met	not met
	Co5	1.66	Male	78	1460	3/3	lung cancer/heart failure	I	28/30	3	0	not met	not met
	Co6	5.5	Male	89	1275	3/3	respiratory distress/COPD	II	30/30	3	0	not met	not met
	Co7	4.75	Male	86	1400	3/3	cardiac arrest	I	28/30	24	0	not met	not met
Mean		3.25	3/4	83.3	1250								
AD	AD1	1.83	Female	84	1080	3/3	end stage AD	VI	0/30	21	C	definite AD	high
	AD2	1.5	Female	85	940	3/3	breast cancer /end stage AD	VI	2/30	28	C	definite AD	high
	AD3	3.16	Male	80	1000	3/4	end stage AD	VI	1/30	12	C	definite AD	high
	AD4	2.25	Male	78	1120	3/4	end stage AD	VI	7/30	12	C	definite AD	high
	AD5	2.5	Male	87	1100	3/2	end stage AD	VI	13/30	12	C	definite AD	high
Mean		2.25	2/3	82.8	1048								

AD, Alzheimer's disease; CERAD, Consortium to Establish a Registry for Alzheimer's Disease; Co, control; MMSE, Mini-Mental State Examination; NIA, National Institute on Aging; PMD, postmortem delay.

paraformaldehyde in 0.1 M phosphate-buffered saline (PBS), pH 7.4 for 3–4 days. Areas containing the regions of interest were cryoprotected in 30% sucrose in 0.1 M PBS, pH 7.4. Series of 30 μm-thick sections were cut on a freezing microtome and collected in PBS containing 0.1% sodium azide.

For biochemical analyses including Aβ ELISAs, QC enzymatic activity assays and quantitative RT-PCR to detect QC transcripts, unfixed temporal cortex tissue with a short *postmortem* interval was stored at −80°C (see Table 1). Brain tissue (10% w/v) was homogenized in TBS (20 mM Tris, 137 mM NaCl, pH 7.6) containing protease inhibitor cocktail (Complete Mini, Roche), sonicated and aliquots of homogenates were used for QC enzymatic activity assays. Homogenates were then centrifuged at 75,500× *g* for 1 hour at 4°C and the supernatant was stored at –80°C. Aβ peptides were sequentially extracted with TBS/1% Triton X-100 (TBS/triton fraction), 2% sodium dodecylsulfate (SDS) in distilled water (SDS fraction), and 70% formic acid (FA fraction). The combined SDS and FA fractions were considered as the insoluble pool of Aβ.

QC and pGlu-Aβ antibodies

Since the specificity of the immunohistochemical QC labeling is critical for this study, we tested four different QC antibodies; 1301 (rabbit anti-QC) and 10269 (goat anti-QC) developed by Probiodrug (Halle, Germany) and the mouse anti-QC antibodies A01 and B01 from Abnova (Heidelberg, Germany). All four antibodies from three different species generated similar staining patterns with a robust cytosolic labeling of layer III pyramidal neurons, indicating specific detection of QC (Fig. 1). Based on the superior signal to background ratio, the mouse anti-QC antibody A01 was selected for the analyses of QC expression in human cortex.

pGlu-Aβ peptides in cortex of AD cases were detected using the mouse monoclonal antibody mab2-48 (Synaptic Systems; Göttingen, Germany), which has been thoroughly characterized by Wirths et al. [42]. This antibody specifically detects the pGlu-Aβ neo-epitope generated by QC activity and does not cross-react with mouse Aβ nor with human $A\beta_{1\text{-}40/42}$ or N-truncated human $A\beta_{3\text{-}40/42}$ lacking the pGlu modification. When required for double labeling procedures (see below), a rabbit anti-pGlu-Aβ antiserum (Synaptic Systems) was used. The rabbit anti-pGlu-Aβ and mouse anti-pGlu-Aβ antibodies showed an identical staining pattern of human brain tissue (not shown).

Immunohistochemistry for human brain tissue

Nissl staining

Coronal sections of the human hippocampus were mounted on gelatin-coated slides and stained in 0.1% cresyl violet according to standard protocols.

Single labeling QC immunohistochemistry

All immunohistochemical procedures were performed on free-floating brain sections. Immunohistochemistry to detect QC in human brain was performed using the mouse anti-QC antiserum A01 (Abnova; 1:2,000). All sections were pre-treated with an initial antigen retrieval step by heating to 90°C in 0.1 M citrate buffer, pH 2.5, for 3 minutes followed by rinsing with PBS; pH 7.4 containing 0.05% Tween (PBS-T). Brain sections were further treated with 2% H_2O_2 in 60% methanol for 1 hour, to abolish endogenous peroxidase activity. Unspecific staining was blocked in PBS-T containing 2% bovine serum albumin (BSA), 0.3% milk powder, and 0.5% normal donkey serum before incubating brain sections with the primary anti-QC antibody at 4°C overnight. The following day sections were incubated with secondary biotinylated donkey anti-mouse antibodies (Dianova; 1:1,000) for 60 minutes at room temperature followed by the ABC method which comprised incubation with complexed streptavidin-biotinylated horseradish peroxidase. Incubations were separated by washing steps (3-times 5 minutes in PBS-T). Binding of peroxidase was visualized by incubation with 2 mg 3,3′-diaminobenzidine (DAB), 20 mg nickel ammonium sulfate, and 2.5 μl H_2O_2 per 5 ml Tris buffer (0.05 M; pH 8.0) for 1–2 minutes, resulting in black labeling.

Sections from control and AD cases were processed in parallel with the same washing, antibody, and staining solutions for the same period of time to prevent technical staining differences.

Double labeling immunohistochemistry

Simultaneous immunohistochemical labeling of QC and pGlu-Aβ was performed using mouse anti-QC (A01, 1:2,000; Abnova) and rabbit anti-pGlu-Aβ (Synaptic Systems; 1:500) antibodies. As for single labeling, all sections were pre-treated with 2% H_2O_2 in 60% methanol for 60 minutes and unspecific staining was blocked by treatment with PBS-T containing 2% BSA, 0.3% milk powder, and 0.5% normal donkey serum before incubating brain sections with the primary antibodies in blocking solution at 4°C for 24 hours. Thereafter, the tissue was transferred

to a mixture of blocking solution and PBS-T buffer (1:2) containing secondary biotinylated donkey anti-mouse antibody (Dianova; 1:400) followed by incubation with extravidin-conjugated peroxidase (Sigma-Aldrich, Germany; 1:2,000) in blocking solution and PBS-T buffer (1:3) for 60 minutes at room temperature. Binding of peroxidase was visualized in a solution containing 4 mg DAB, 40 mg ammonium nickel(II)-sulfate, and 5 μl H_2O_2 per 10 ml Tris-buffer (0.05 M; pH 8.0) yielding black epitope staining. Bound peroxidase was then inactivated with 2% H_2O_2 in 60% methanol (15 minutes) to allow subsequent detection of pGlu-Aβ with a peroxidase-labeled donkey anti-rabbit antibody (Dianova; 1:200; 60 minutes) followed by visualization of second round peroxidase binding with 2 mg DAB and 2.5 μl H_2O_2 per 5 ml Tris buffer (0.05 M; pH 7.6) resulting in a brown precipitate.

Quantification of QC-immunoreactive neurons

Quantitative analysis of QC-immunoreactive neurons present in temporal and entorhinal cortex was performed. Neurons were counted when a minimum soma diameter of 8 μm and at least one dendrite could be identified. The location of neurons throughout all cortical layers from the cortical surface to the white matter boundary was assessed by means of the optical fractionator method. In the present investigation, the number of QC-positive neurons was counted in discrete neocortical areas of temporal cortex (area 22) and entorhinal cortex (area 28) of six control brains and six cases with a neuropathologically-confirmed diagnosis of AD. Counts were performed on a Zeiss Axioskop 2 plus microscope equipped with a motorized stage, a Ludl MAC 5000 (LEP, Hawthorne, NY, USA) and a digital camera 9000 (MicroBrightField, Williston, VT, USA). Stereo Investigator software 7 (MicroBrightfield) was used to analyze frontal sections (nominal thickness of 30 μm) of selected areas. Each section was first viewed at low magnification (5×) for outlining the relevant parts of cortical areas, and disector frames were placed in a systematic-consecutive fashion in the delineated regions of the sections. Neurons that fell within these disector frames (250 μm × 1000 μm) were then counted at high magnification (10×). On average, the post-processing shrinkage of the tissues resulted in a final section thickness of about 16 μm, which permitted a consistent sampling of 10 μm with the dissector and the use of guard zones of 2 μm on either sides of the section. Three sections per case and area investigated were used. The number of QC-positive neurons was converted to numerical density per mm^2 and is given as mean ± SD of 6 control and 6 AD cases.

Cells were considered to be immunoreactive when they were clearly visible at the settings: brightness −0.5; contrast 2.5; and gamma 1.6. Neurons were assigned to the strongly QC-immunoreactive group, when the soma was clearly above background at the threshold settings brightness 2.0; contrast 10.0; and gamma 3.0. In consecutive brain sections, the total number of neurons was calculated by Nissl staining and was set to represent 100% of neurons. The relative numbers of QC-immunoreactive neurons in brain regions analyzed was calculated using the formula of Konigsmark [43].

qRT-PCR for QC

Tissue samples were homogenized by means of the homogenizer Precellys with 1.4 mm ceramic beads (5000 rpm, 30 seconds, Peqlab). RNA was isolated using the NucleoSpin RNA II kit (Macherey Nagel) according to the manufacturer's instructions. The quality of isolated RNA was validated by calculating the ratio of absorbance at 260 and 280 nm, which was consistently above 2. RNA concentrations were measured using a NanoDrop 2000 spectrophotometer (Peqlab) and 0.1 μg RNA was reverse transcribed into cDNA using random primers (Roche) and Superscript III (Life technologies). Quantitative PCR was performed in a Rotorgene3000 (Corbett Research) using the Rotor-Gene SYBR Green PCR kit and the Quantitect primer assays HsQPCT (Qiagen). Relative amounts of gene expression were determined with the Rotorgene software version 6.1 in comparative quantitation mode. Normalization was done against the stably expressed reference gene YWHAZ identified using Normfinder [44]. The PCR was verified by product melting curves and single amplicons were confirmed by agarose gel electrophoresis.

QC enzymatic activity assays

QC activity was measured by a discontinuous HPLC-method using the substrate H-Gln-βNA as described previously [27]. Briefly, QC-containing tissue lysate was incubated with substrate H-Gln-βNA. Test samples were taken at defined time points and the reaction was stopped by boiling for 5 minutes. Analysis of pGlu-βNA formation was done using RP18 LiChroCART HPLC Cartridge and the HPLC-system D-7000 (Merck-Hitachi). QC activity was quantified from a standard curve of pGlu-βNA under assay conditions.

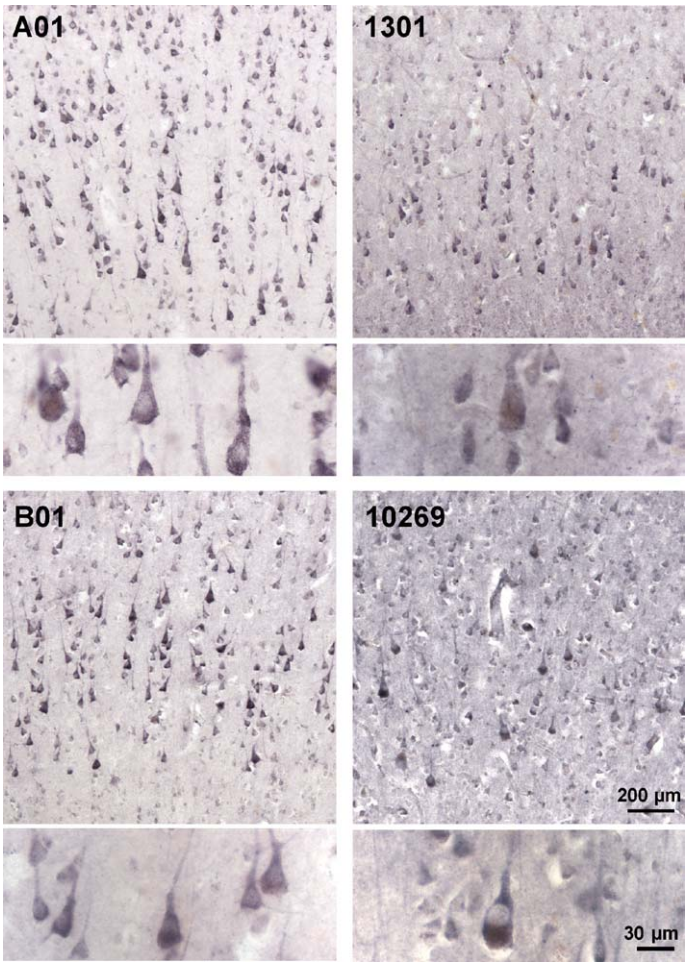

Fig. 1. Characterization of QC antibodies. Immunohistochemical detection of neurons in consecutive brain sections of Area 22 of a human control case using four different anti-QC antibodies as indicated. All antibodies primarily detect QC in the cytosol and in neurites; in particular in strongly immunoreactive pyramidal neurons in layer III. The 200 µm scale bar applies to all low magnification images; the 30 µm scale bar applies to all high magnification images.

Aβ ELISAs

Specific ELISAs to detect $A\beta_{x\text{-}42}$ and pGlu-$A\beta_{3\text{-}42}$ (IBL, Hamburg) were performed according to the manufacturer's manual as described by Schilling et al. [29]. All samples were analyzed in triplicate and the concentrations of the respective Aβ peptides present in temporal cortex were calculated from a standard curve.

Statistical analyses

Data on the number of QC-immunoreactive neurons in temporal and entorhinal cortex are the mean value of 6 control and 6 AD cases ± SD. For biochemical measurements and correlation analyses brain tissue from 7 control and 5 AD cases was used.

The ELISA data have been evaluated applying non-parametric Mann-Whitney tests.

RESULTS

Characterization of QC antibodies in human cortex

In order to determine the specificity of the immunohistochemical QC labeling in human cortex, four different QC antibodies raised in three species were characterized. All antibodies labeled a significant proportion of neocortical neurons with the most robust staining intensity in layer III pyramidal neurons (Fig. 1). At higher magnification, a localization of QC immunoreactivity in cytoplasm and dendrites was

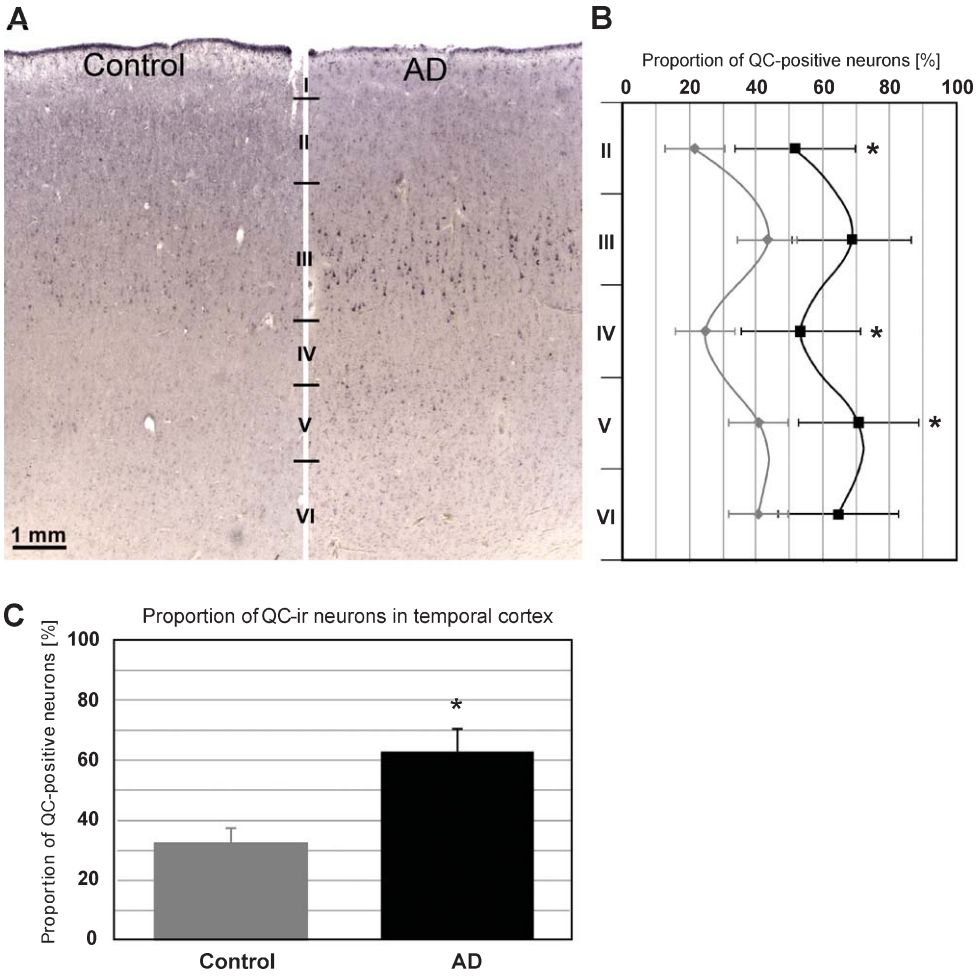

Fig. 2. Density of QC-immunoreactive neurons in human temporal cortex. A) The typical staining pattern for QC in *postmortem* human temporal cortex of a control case and an AD case is shown. Note the strong QC immunoreactivity in layer III. B) The laminar distribution of QC immunoreactive neurons is given as per cent of the total neuron number quantified by Nissl staining. The highest density of QC-immunoreactive neurons was detected in layers III and V of control and AD cases with a 20 to 30% higher frequency across all layers in AD. C) Quantification of the percentage of QC-immunoreactive neurons in control and AD cases across the cortical thickness from layer II to VI. The percentage of QC-immunoreactive neurons is twice as high in AD as compared to the age-matched control group. $*p < 0.0001$; Data are mean values $\pm$ SD; Control: $n = 6$; AD: $n = 6$.

evident. Although all antibodies labeled the same neuronal populations and revealed a similar subcellular QC distribution, there were considerable differences in the signal to background ratio, with A01 showing the best staining characteristics (Fig. 1). Therefore, this antibody was used for subsequent analyses of QC expression in human control and AD brains.

QC expression in temporal cortex

In the temporal cortex, a defined laminar distribution of QC immunoreactivity was observed (Fig. 2A). In control cases, approximately 20 to 25% of neurons in layers II and IV displayed QC immunoreactivity, whereas 40 to 45% of neurons in layers III, V, and VI were found to be QC-immunoreactive (Fig. 2B). In AD, a similar laminar profile of QC immunoreactivity was detected but the proportion of QC-immunoreactive neurons was 20 to 30% higher in all cortical layers compared to controls (Fig. 2A, B). This increase was statistically significant in layers II, IV, and V ($p < 0.05$). Quantification of QC immunoreactive neurons over the whole cortical depth revealed a proportion of $31.5 \pm 5.0\%$ QC-immunoreactive neurons in control brains and of $61.7 \pm 7.8\%$ in AD brains (Fig. 2C; $p < 0.0001$).

As stated above, the QC staining intensity varied considerably between individual neurons. To take into

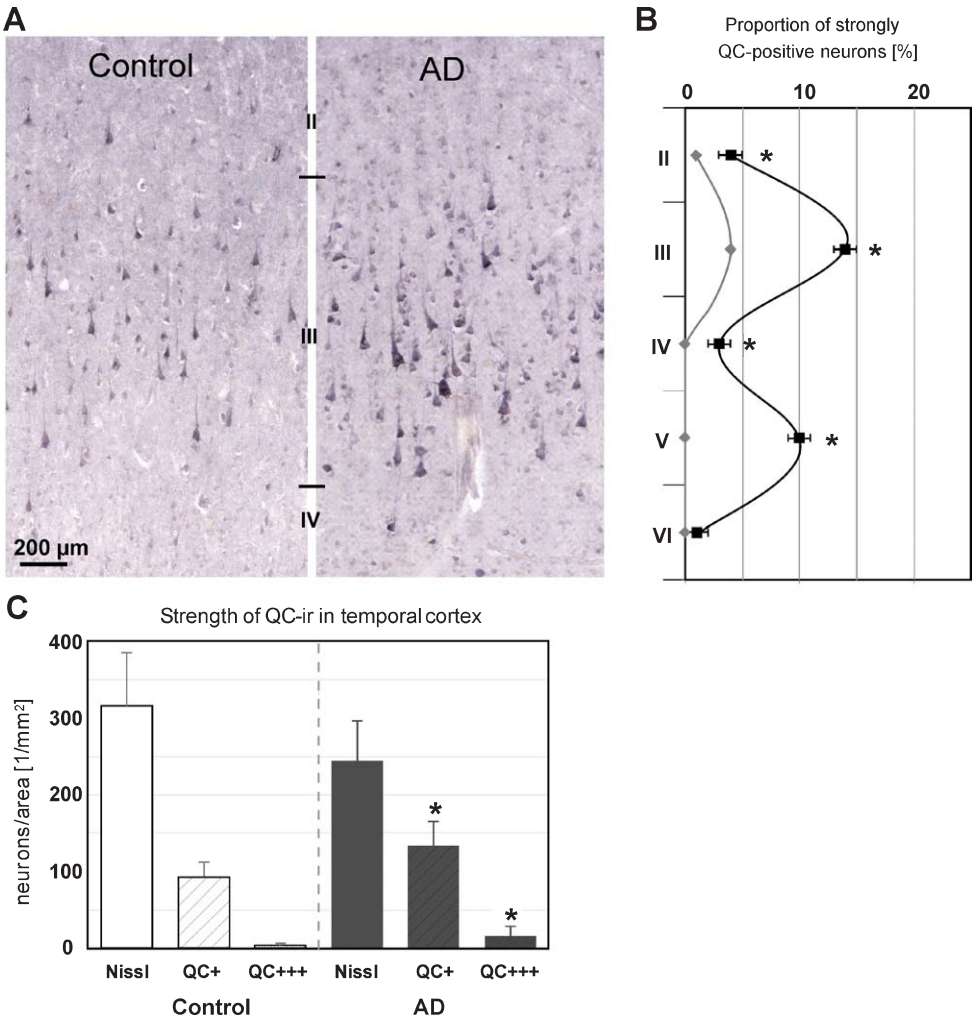

Fig. 3. Strength of the QC immunoreactivity in temporal cortex neurons. A) The immunohistochemical labeling of QC reveals remarkable differences in the staining intensity of individual neurons between control and AD cases. B) Quantification of strongly QC-immunoreactive neurons demonstrates the presence of a minor proportion of such neurons only in cortical layer III of control cases, but in all cortical layers of AD cases. The highest proportion of strongly QC-immunoreactive neurons in AD was detected in layers III and V. C) Quantification of strongly and moderately QC-immunoreactive neurons identifies statistically significant increases in the proportion of both groups of QC neurons in AD. *$p < 0.05$; Data are mean values ± SD; Control: $n = 6$; AD: $n = 6$.

account this variation, a second analysis differentiating between strongly and moderately QC-immunoreactive neurons in temporal cortex was performed (Fig. 3). In controls, 93 ± 20 neurons/mm^2 displayed a moderate and 3 ± 3 neurons/mm^2 showed a strong QC immunoreactivity (Fig. 3C). In AD temporal cortex, the number of both moderately (133 ± 32) and strongly (16 ± 12) QC immunoreactive neurons per mm^2 was significantly higher than in controls (Fig. 3C; $p < 0.05$). Neurons with strong QC immunoreactivity were exclusively found in layer III of control and in layers III and V as well as to a lesser extent in layers II and IV of AD temporal cortex (Fig. 3B). In all cortical layers with strongly QC-immunoreactive neurons their proportion was significantly higher in AD than in control brains (Fig. 3B; $p < 0.01$).

QC expression in entorhinal cortex

We further compared the QC expression in temporal cortex with the one of entorhinal cortex, which is earlier and more severely affected in the course of AD. In contrast to temporal cortex, entorhinal cortex has a different morphology and layering. In the entorhinal cortex of control cases, more than 80% of neurons displayed QC immunoreactivity, with the strongest

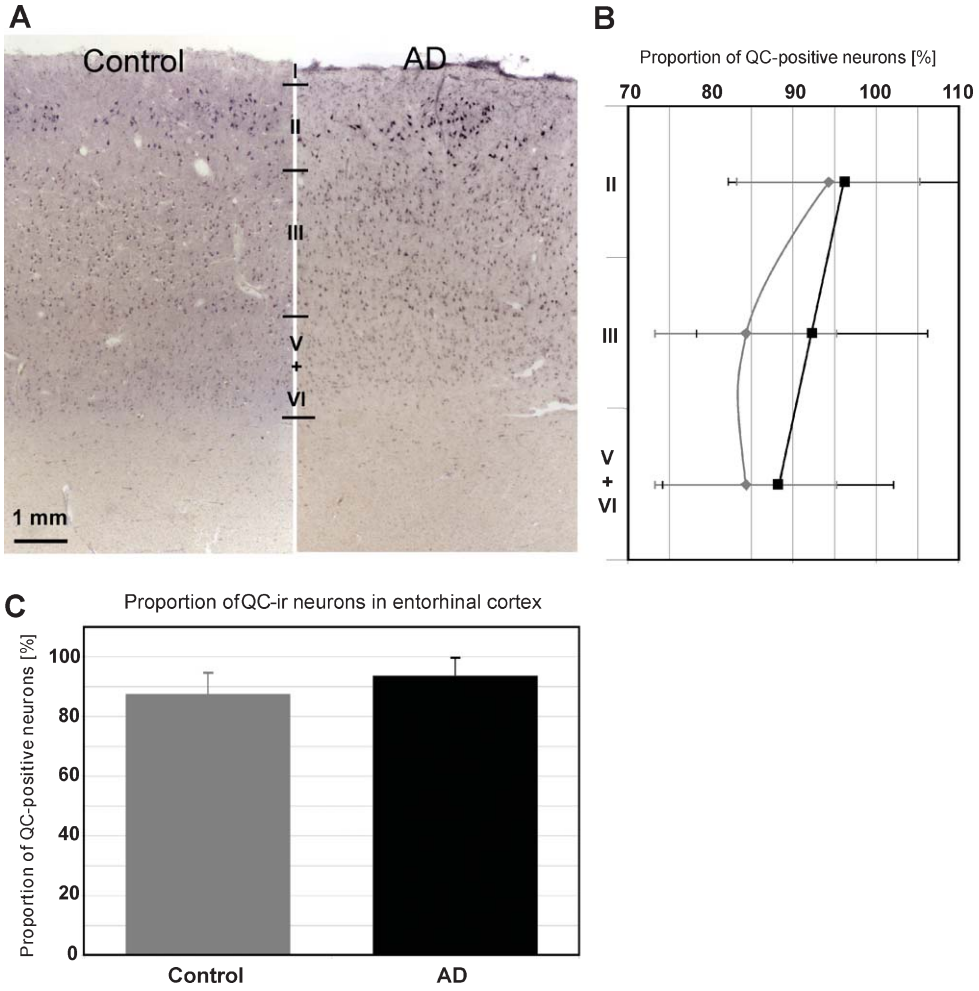

Fig. 4. Density of QC-immunoreactive neurons in human entorhinal cortex. A) A representative staining pattern for QC in postmortem human entorhinal cortex of a control case and an AD case is shown. Note the strong QC immunoreactivity in the islands of layer II and in layer III of the entorhinal cortex. B) The laminar distribution of QC immunoreactive neurons is given as per cent of the total neuron number quantified by Nissl staining. The highest density of QC-immunoreactive neurons was detected in layer II with a gradient toward a lower proportion of QC-immunoreactive neurons in deeper cortical layers. Already in the control group, 85 to 95% of the neurons expressed QC. There was no statistically significant increase in the density of QC-immunoreactive neurons in any of the entorhinal cortex layers. C) Quantification of the percentage of QC-immunoreactive neurons in control and AD cases revealed no differences between the control and the AD group across the cortical thickness from layer II to VI. Data are mean values ± SD; Control: $n = 6$; AD: $n = 6$.

labeling being present in neurons of layer II islands (Fig. 4A, B). In AD entorhinal cortex, a similar staining pattern with approximately 90% QC-immunoreactive neurons and robust labeling of layer II islands was observed (Fig. 4A, B, C). There was no statistically significant increase in the proportion of QC-positive neurons in AD entorhinal cortex compared to controls (Fig. 4C).

However, when considering the QC staining intensity of individual neurons, there was a statistically significant increase in the number of strongly QC-immunoreactive neurons in AD entorhinal cortex ($80 \pm 42/mm^2$) compared to controls ($40 \pm 40/mm^2$) (Fig. 5; $p < 0.05$). This increase in strongly QC-immunoreactive neurons in AD was for the most part located in layer III (Fig. 5B) and accompanied by a statistically non-significant decrease in the number of moderately QC-immunoreactive neurons in AD ($140 \pm 45/mm^2$) compared to controls ($179 \pm 72/mm^2$) (Fig. 5C).

Co-localization of QC with pGlu-Aβ deposits

Next, we were interested to reveal whether there is a spatial correlation between QC-immunoreactive neurons and pGlu-Aβ deposits in AD cortex. In Fig. 6,

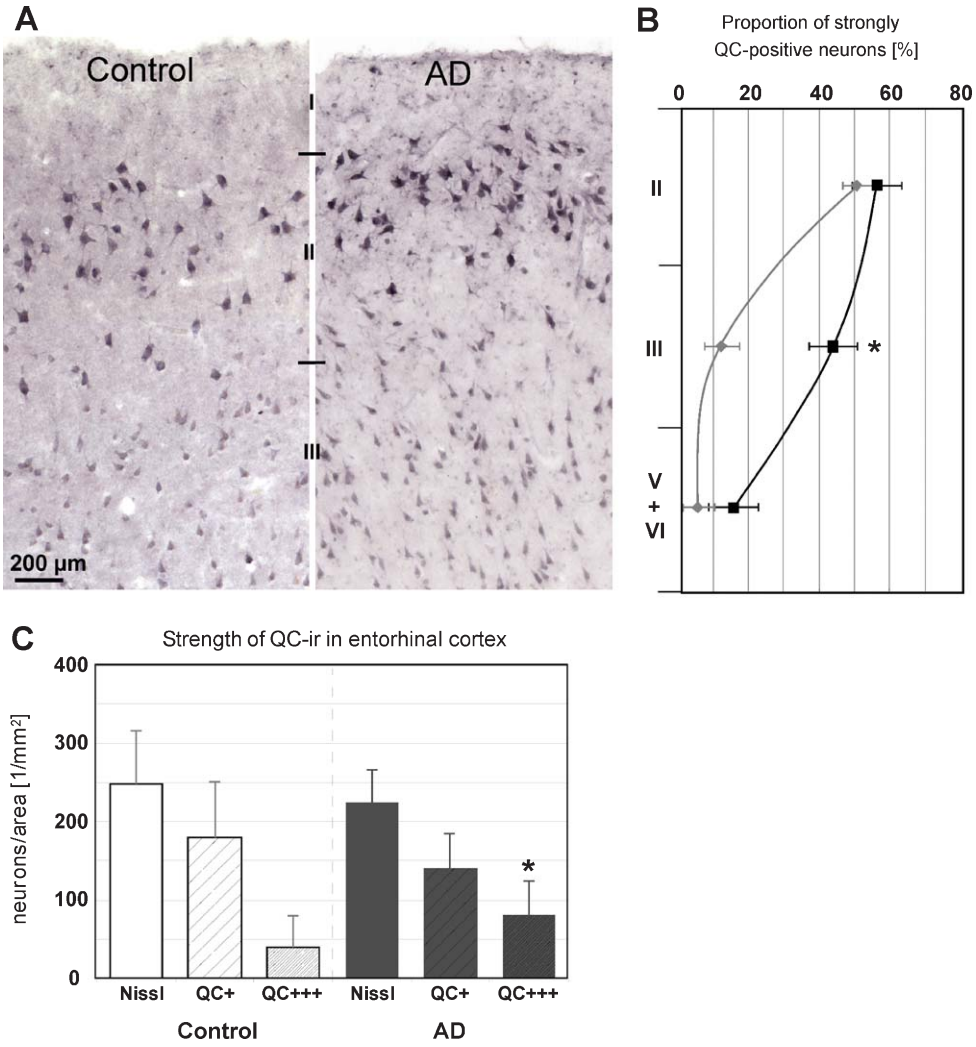

Fig. 5. Strength of the QC immunoreactivity in entorhinal cortex neurons. A) The immunohistochemical labeling of QC reveals differences in the staining intensity of individual neurons between control and AD cases. B) Quantification of strongly QC-immunoreactive neurons demonstrates the presence of such neurons in cortical layer II and to a lesser extent in layers III, V and VI of control cases. In AD cases, there is a higher density of strongly QC-immunoreactive neurons in layer III. C) Quantification of strongly and moderately QC-immunoreactive neurons revealed a statistically significant increase in the proportion of strongly QC-immunoreactive neurons in AD, but a statistically non-significant reduction in the proportion of moderately QC-immunoreactive neurons. *$p < 0.05$; Data are mean values ± SD; Control: $n = 6$; AD: $n = 6$.

an overview of Nissl staining, QC immunohistochemistry, and double labeling for QC (black) and pGlu-Aβ (brown) are shown throughout the entire depth of the temporal cortex. Both QC-immunoreactive neurons and pGlu-Aβ deposits appear to be enriched in layers III and V. However, pGlu-Aβ deposits are also present in layers II and VI, which only harbor a low number of QC immunoreactive neurons. In the high magnification insets on the right panel, examples of a close association of QC-immunoreactive neurons with pGlu-Aβ deposits (middle, bottom) and a lack of such an association (top) are shown. This is consistent with observations made in the hippocampal formation where the appearance of pGlu-Aβ deposits in layers devoid of QC-immunoreactive cell bodies, but enriched with QC immunoreactive afferents from entorhinal cortex, was demonstrated [36].

Quantification of QC mRNA and enzymatic activity and (pGlu)-Aβ in AD

In the second set of human brain tissues, quantitative biochemical analyses were performed with the aims (i) to validate a role of QC in pGlu-Aβ formation in human brain and (ii) to correlate biochemical alterations such as expression of QC and pGlu-Aβ formation with the

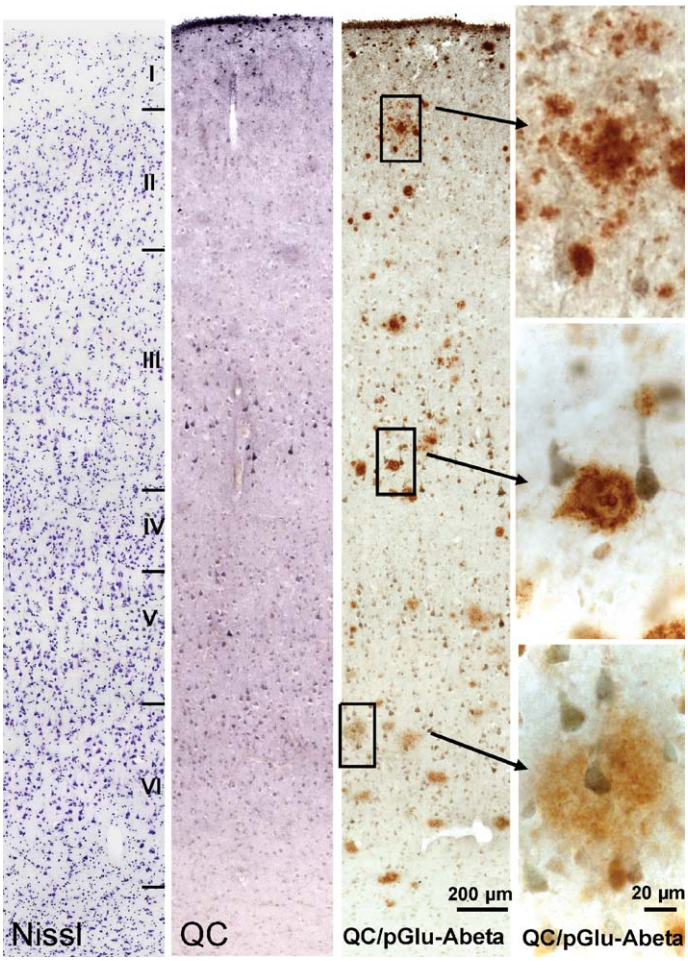

Fig. 6. Spatial association between QC-immunoreactive neurons and pGlu-Aβ deposits. Temporal cortex layers were identified in Nissl-stained brain sections (left). The labeling of QC-immunoreactive neurons (second image from left) demonstrates the highest density of QC in pyramidal neurons in layers III and V. The pGlu-Aβ deposits (brown) were detected in these cortical layers but also layers with a lower abundance of QC-immunoreactive neurons (black) in double labelings (second image from right). In the high magnification images (right), examples of an association between QC-immunoreactive neurons and pGlu-Aβ deposits (bottom, middle) and of a lack of such an association (top) are shown.

test results of MMSE. To address this issue, pathologically and clinically well-characterized brain samples with a short postmortem interval were used (Table 1). In this set of experiments we focused on temporal cortex because entorhinal cortex already showed very high QC expression in controls and no significant increase at the end stage of AD. By using qRT-PCR, an increase in QC mRNA levels by $88.7 \pm 42.6\%$ in AD temporal cortex compared to controls was detected (Fig. 7A; $p < 0.05$). There was also a tendency toward increased enzymatic QC activity in AD, which failed to reach statistical significance (Fig. 7A; increase by $31.6 \pm 35.1\%$; $p > 0.05$).

Consistent with our previous observations [30], this AD cohort also displayed significantly higher pGlu-Aβ (25-fold) and $A\beta_{x-42}$ (70-fold) concentrations compared to the control cases (Fig. 7B; $p < 0.0001$).

Correlation of QC mRNA levels with pGlu-Aβ and MMSE

In order to validate a role of QC in pGlu-Aβ formation of human brain and in cognitive decline in AD, a series of correlation analyses comparing biochemical and clinical parameters from individual control and AD cases was performed.

Firstly, in order to corroborate the role of QC in pGlu-Aβ formation in human brain, the individual QC mRNA levels were plotted versus pGlu-Aβ and unmodified Aβ concentrations. There was a fairly good correlation between QC mRNA and pGlu-Aβ

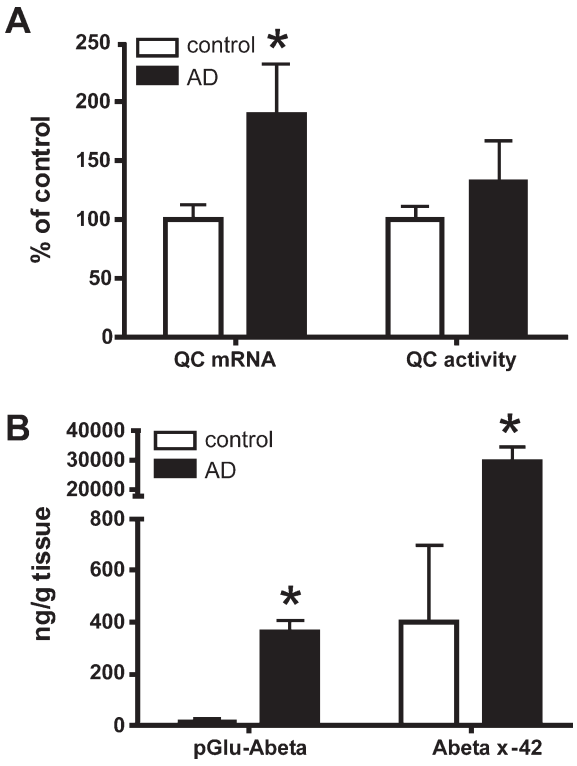

Fig. 7. Alterations in QC expression, Aβ, and pGlu-Aβ peptide concentrations in AD. A) The QC mRNA levels as well as QC enzymatic activity were quantified in temporal cortex samples from control and AD cases. While the increase in QC mRNA levels in AD was statistically significant, the higher enzymatic activity was not. B) Quantification of the insoluble pool of pGlu-Aβ and $Aβ_{x-42}$ in control and AD cases. The concentrations of both Aβ peptide species were significantly increases in AD. $*p < 0.05$.

($r = 0.6386$; $p = 0.0254$; Fig. 8A). Such a correlation did not exist between QC mRNA levels and unmodified Aβ peptide concentrations (Fig. 8B), substantiating a role of QC in pGlu-Aβ formation in human brain.

Secondly, another important question we sought to address was a possible correlation between (pGlu)-Aβ load and MMSE. As expected, both higher concentrations of unmodified Aβ ($r = –0.8263$; $p = 0.0009$; Fig. 8D) and of pGlu-Aβ ($r = –0.8867$; $p = 0.0001$; Fig. C) showed strong and statistically highly significant correlations with a decline in MMSE, which was, however, almost one order of magnitude higher for pGlu-Aβ in the p value.

DISCUSSION

This is the first demonstration of a correlation between the clinical status of elderly human subjects as assessed by MMSE on the one hand and the expression of QCs and the concentration of pGlu-Aβ aggregates on the other hand. The presence of pGlu-Aβ in brains of AD patients is known since the mid-1990s [8, 21], but their generation by QC [26] and their pathogenic profiles [12, 13, 24] have only been discovered in the last decade. Interestingly, both QC and pGlu-Aβ were demonstrated to be enriched in subcortical and hippocampal structures known to be severely affected in AD [35, 37]. Because of the high aggregation propensity, the seeding capacity to induce deposition of unmodified Aβ peptides and their neurotoxicity, pGlu-Aβ peptides appear as a novel target for AD therapy. Both, prevention of pGlu-Aβ formation by inhibition of QC [29] and removal of pGlu-Aβ aggregates by immunization [45–47] have been demonstrated to be feasible therapeutic strategies in transgenic mouse models. A currently completed phase I clinical trial demonstrated the safety and efficiency of the QC inhibitor PQ912 in healthy humans [48].

However, there is still a lack of data correlating the clinical status of elderly humans with QC expression levels and pGlu-Aβ deposits in brain. To address this issue, we first analyzed QC expression in two cortical areas differentially affected in AD. Temporal cortex (Area 22) is part of the associative cortex involved in language processing [49] and affected at later stages of the disease, while entorhinal cortex (Area 28) is vital for spatial memory formation and consolidation [50, 51] and one of the earliest and most severely affected brain region in AD [4, 52].

Here, we report a widespread expression of QC by temporal cortex neurons in human control subjects. Given the substrate specificity of QC for peptide hormones and neuropeptides present in hypothalamus and in pituitary gland and the involvement of QC in pathogenic pGlu-Aβ formation, this observation was unexpected. Such a high QC expression by cortical neurons of control subjects calls for an investigation of currently unknown physiological QC substrates in cortex. On the other hand, the upregulation of QC expression in temporal cortex of AD patients is in line with the postulated role for QC in AD pathogenesis. Both QC mRNA and protein levels have been already reported to be upregulated at early stages of AD in neocortex [29], hippocampus [53], and peripheral blood cells [54], and there is evidence for a role of disturbed calcium homeostasis in the regulation of QC expression [53]. The frequent association of QC-immunoreactive neurons with pGlu-Aβ deposits in cortical layers III and V is also supportive for a pathogenic role of QC.

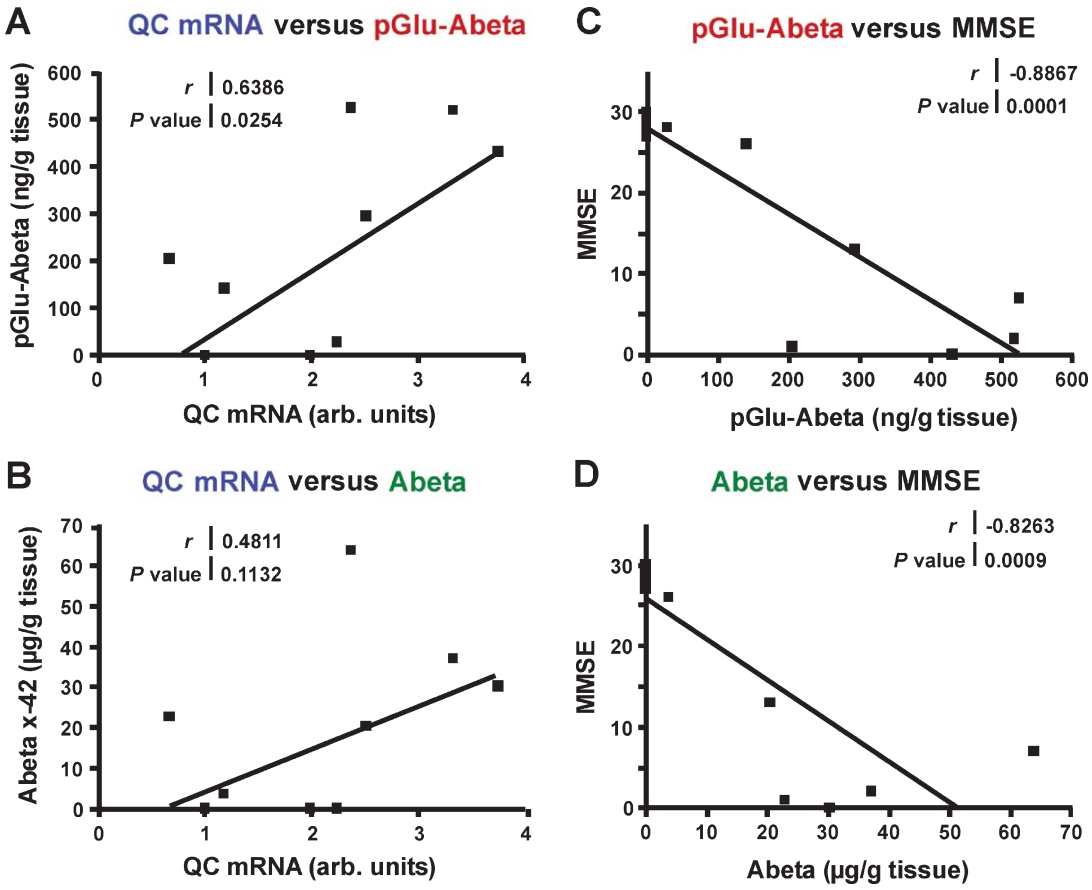

Fig. 8. Correlations between QC mRNA levels, Aβ peptide concentrations, and MMSE. There was a statistically significant correlation between QC mRNA and pGlu-Aβ (A; $r = 0.6386$; $p = 0.0254$). Such a correlation did not exist between QC mRNA levels and unmodified Aβ peptide concentrations (B). Both higher concentrations of pGlu-Aβ (C; $r = –0.8867$; $p = 0.0001$) and of unmodified Aβ (D; $r = –0.8263$; $p = 0.0009$) showed strong correlations with a decline in MMSE which was one order of magnitude higher for pGlu-Aβ. Control: $n = 7$; AD: $n = 5$.

There are, however, cortical pGlu-Aβ deposits in layers II and VI that are not obviously associated with QC-immunoreactive neuronal somata. Such a phenomenon has been reported earlier in the hippocampal formation [37] and is most likely due to release of pGlu-Aβ from synaptic terminals of QC-rich neurons. This may include intracortical neurons such as pyramidal neurons and afferents from QC-rich structures like locus coeruleus and nucleus basalis Meynert, which have been reported to express high levels of QC and are affected by pGlu-Aβ pathology in AD [35]. Such a "seeding from the distance" of Aβ deposits by subcortical neurons has been discussed to contribute to the development of AD pathology [55]. Furthermore, in an AβPP transgenic mouse model, the seeding of Aβ deposits in brain structures lacking transgene expression has been shown to occur via synaptic Aβ release from projection neurons [56]. The even higher expression of QC in entorhinal cortex might explain the particularly high vulnerability of this neuronal population in AD.

Since QC expression in temporal cortex displayed higher differences between control and AD than entorhinal cortex, the former brain region was used for thorough biochemical and clinical analyses. Brain tissue with a very short *postmortem* delay and a well-documented clinical status was received from the Bannerhealth Brain Donation Program used for biochemical analyses including qRT-PCR to detect QC mRNA, QC enzymatic activity assays and ELISA to quantify Aβ and pGlu-Aβ concentrations. QC transcript levels were shown to be elevated in AD temporal cortex, as were insoluble Aβ and pGlu-Aβ concentrations.

For individual cases, biochemical values were correlated with cognitive status as measured by MMSE. Here, a good correlation between QC mRNA levels and the concentration of pGlu-Aβ—but not total Aβ—was

detected. This provides further evidence for the specificity of QC for pGlu-Aβ formation in human cortex. There were also robust inverse correlations between Aβ concentrations and MMSE. This is not surprising since both peptide aggregates are characteristic of AD. However, the *p* value was one order of magnitude higher for the pGlu-Aβ/MMSE correlation than for the Aβ/MMSE correlation. This points toward a specific role of pGlu-Aβ in cognitive decline in AD and underlines the therapeutic potential of targeting pGlu-Aβ by inhibition of QC and by immunization approaches. Since the sample size investigated in the present study is not high and cases with a moderate decline in MMSE are of particular interest for correlation analyses, we are looking forward to additional studies that further strengthen the key findings reported here.

Together, our observations provide evidence for an involvement of QC in AD pathogenesis by QC-catalyzed pGlu-Aβ formation which affects cognitive abilities.

ACKNOWLEDGMENTS

We are grateful to the Banner Sun Health Research Institute Brain Donation Program of Sun City, Arizona for the provision of human brain tissue. The Brain Donation Program is supported by the National Institute on Aging [P30 AG19610 Arizona Alzheimer's Disease Core Center], the Arizona Department of Health Services [contract 211002, Arizona Alzheimer's Research Center], the Arizona Biomedical Research Commission [contracts 4001, 0011, 05-901, and 1001 to the Arizona Parkinson's Disease Consortium], and the Michael J. Fox Foundation for Parkinson's Research. We thank R. Jendrek (Paul Flechsig Institute for Brain Research), K. Schulz and E. Scheel (Probiodrug) for technical assistance. This work was supported by the German Federal Department of Education, Science and Technology, BMBF [grant #0316033A to HUD and grant #0316033B to SR]. Further, this work was supported by the German Research Foundation MO 2249/2-1 within the SPP 1608, GRK 1097 "INTERNEURO" to MM, by the COST Action BM1001 "Brain Extracellular Matrix in Health and Disease" to MM, by the Alzheimer Forschungsinitiative e.V. (AFI #11861 to MM) and by the European Union and the Federal State of Saxony (grant number SAB 100154907) to MM and SR.

Authors' disclosures available online (http://www.j-alz.com/disclosures/view.php?id=1956).

REFERENCES

[1] Maeda J, Zhang MR, Okauchi T, Ji B, Ono M, Hattori S, Kumata K, Iwata N, Saido TC, Trojanowski JQ, Lee VM, Staufenbiel M, Tomiyama T, Mori H, Fukumura T, Suhara T, Higuchi M (2011) *In vivo* positron emission tomographic imaging of glial responses to amyloid-beta and tau pathologies in mouse models of Alzheimer's disease and related disorders. *J Neurosci* **31**, 4720-4730.

[2] Leung KK, Bartlett JW, Barnes J, Manning EN, Ourselin S, Fox NC; Alzheimer's Disease Neuroimaging Initiative (2013) Cerebral atrophy in mild cognitive impairment and Alzheimer disease: Rates and acceleration. *Neurology* **80**, 648-654.

[3] Schuitemaker A, Kropholler MA, Boellaard R, van der Flier WM, Kloet RW, van der Doef TF, Knol DL, Windhorst AD, Luurtsema G, Barkhof F, Jonker C, Lammertsma AA, Scheltens P, van Berckel BN (2013) Microglial activation in Alzheimer's disease: An (R)-[^{11}C]PK11195 positron emission tomography study. *Neurobiol Aging* **34**, 128-136.

[4] Braak H, Braak E (1991) Neuropathological stageing of Alzheimer-related changes. *Acta Neuropathol* **81**, 239-259.

[5] Mirra SS, Heyman A, McKeel D, Sumi SM, Crain BJ, Brownlee LM, Vogel FS, Hughes JP, van Belle G, Berg L (1991) The Consortium to Establish a Registry for Alzheimer's Disease (CERAD). Part II. Standardization of the neuropathologic assessment of Alzheimer's disease. *Neurology* **41**, 479-486.

[6] Selkoe DJ, Schenk D (2003) Alzheimer's disease: Molecular understanding predicts amyloid based therapeutics. *Annu Rev Pharmacol Toxicol* **43**, 545-584.

[7] Haass C (2004) Take five-BACE and the gamma-secretase quartet conduct Alzheimer's amyloid beta-peptide generation. *EMBO J* **23**, 483-488.

[8] Saido TC, Iwatsubo T, Mann DM, Shimada H, Ihara Y, Kawashima S (1995) Dominant and differential deposition of distinct beta-amyloid peptide species, Abeta N3(pE), in senile plaques. *Neuron* **14**, 457-466.

[9] Saido TC, Yamao H, Iwatsubo T, Kawashima S (1996) Amino- and carboxyl-terminal heterogeneity of beta-amyloid peptides deposited in human brain. *Neurosci Lett* **215**, 173-176.

[10] Russo C, Schettini G, Saido TC, Hulette C, Lippa C, Lannfelt L, Ghetti B, Gambetti P, Tabaton M, Teller JK (2000) Presenilin-1 mutations in Alzheimer's disease. *Nature* **405**, 531-532.

[11] Sevalle J, Amoyel A, Robert P, Fournié-Zaluski MC, Roques B, Checler F (2009) Aminopeptidase A contributes to the N-terminal truncation of amyloid beta-peptide. *J Neurochem* **109**, 248-256.

[12] Miravalle L, Calero M, Takao M, Roher AE, Ghetti B, Vidal R (2005) Amino-terminally truncated Abeta peptide species are the main component of cotton wool plaques. *Biochemistry* **44**, 10810-10821.

[13] Piccini A, Russo C, Gliozzi A, Relini A, Vitali A, Borghi R, Giliberto L, Armirotti A, D'Arrigo C, Bachi A, Cattaneo A, Canale C, Torrassa S, Saido TC, Markesbery W, Gambetti P, Tabaton M (2005) Beta-amyloid is different in normal aging and in Alzheimer's disease. *J Biol Chem* **280**, 34186-34192.

[14] Portelius E, Bogdanovic N, Gustavsson MK, Volkmann I, Brinkmalm G, Zetterberg H, Winblad B, Blennow K (2010) Mass spectrometric characterization of brain amyloid beta isoform signatures in familial and sporadic Alzheimer's disease. *Acta Neuropathol* **120**, 185-193.

[15] He W, Barrow CJ (1999) The A beta 3-pyroglutamyl and 11-pyroglutamyl peptides found in senile plaque have greater

beta-sheet forming and aggregation propensities *in vitro* than full-length A beta. *Biochemistry* **38**, 10871-10877.

[16] Russo C, Violani E, Salis S, Venezia V, Dolcini V, Damonte G, Benatti U, D'Arrigo C, Patrone E, Carlo P, Schettini G (2002) Pyroglutamate-modified amyloid beta-peptides – AbetaN3(pE) – strongly affect cultured neuron and astrocyte survival. *J Neurochem* **82**, 1480-1489.

[17] Schilling S, Lauber T, Schaupp M, Manhart S, Scheel E, Böhm G, Demuth HU (2006) On the seeding and oligomerization of pGlu-amyloid peptides (*in vitro*). *Biochemistry* **45**, 12393-12399.

[18] Schlenzig D, Manhart S, Cinar Y, Kleinschmidt M, Hause G, Willbold D, Funke SA, Schilling S, Demuth HU (2009) Pyroglutamate formation influences solubility and amyloidogenicity of amyloid peptides. *Biochemistry* **48**, 7072-7078.

[19] D'Arrigo C, Tabaton M, Perico A (2009) N-terminal truncated pyroglutamyl beta amyloid peptide Abetapy3-42 shows a faster aggregation kinetics than the full-length Abeta1-42. *Biopolymers* **91**, 861-873.

[20] McColl G, Roberts BR, Gunn AP, Perez KA, Tew DJ, Masters CL, Barnham KJ, Cherny RA, Bush AI (2009) The Caenorhabditis elegans Aβ1-42 model of Alzheimer's disease predominantly expresses Aβ3-42. *J Biol Chem* **284**, 22697-22702.

[21] Saido TC (1998) Alzheimer's disease as proteolytic disorders: Anabolism and catabolism of beta-amyloid. *Neurobiol Aging* **19**, S69-S75.

[22] Acero G, Manutcharian K, Vasilevko V, Munguia ME, Govezensky T, Coronas G, Luz-Madrigal A, Cribbs DH, Gevorkian G (2009) Immunodominant epitope and properties of pyroglutamate-modified Aβ-specific antibodies produced in rabbits. *J Neuroimmunol* **213**, 39-46.

[23] Wirths O, Breyhan H, Cynis H, Schilling S, Demuth HU, Bayer TA (2009) Intraneuronal pyroglutamate-Abeta 3-42 triggers neurodegeneration and lethal neurological deficits in a transgenic mouse model. *Acta Neuropathol* **118**, 487-496.

[24] Nussbaum JM, Schilling S, Cynis H, Silva A, Swanson E, Wangsanut T, Tayler K, Wiltgen B, Hatami A, Rönicke R, Reymann K, Hutter-Paier B, Alexandru A, Jagla W, Graubner S, Glabe CG, Demuth HU, Bloom GS (2012) Prion-like behaviour and tau-dependent cytotoxicity of pyroglutamylated amyloid-β. *Nature* **485**, 651-655.

[25] Maeda J, Ji B, Irie T, Tomiyama T, Maruyama M, Okauchi T, Staufenbiel M, Iwata N, Ono M, Saido TC, Suzuki K, Mori H, Higuchi M, Suhara T (2007) Longitudinal, quantitative assessment of amyloid, neuroinflammation, and anti-amyloid treatment in a living mouse model of Alzheimer's disease enabled by positron emission tomography. *J Neurosci* **27**, 10957-10968.

[26] Schilling S, Hoffmann T, Manhart S, Hoffmann M, Demuth HU (2004) Glutaminyl cyclases unfold glutamyl cyclase activity under mild acid conditions. *FEBS Lett* **563**, 191-196.

[27] Cynis H, Schilling S, Bodnar M, Hoffmann T, Heiser U, Saido TC, Demuth HU (2006) Inhibition of glutaminyl cyclase alters pyroglutamate formation in mammalian cells. *Biochim Biophys Acta* **1764**, 1618-1625.

[28] Cynis H, Scheel E, Saido TC, Schilling S, Demuth HU (2008) Amyloidogenic processing of amyloid precursor protein: Evidence of a pivotal role of glutaminyl cyclase in generation of pyroglutamate-modified amyloid-beta. *Biochemistry* **47**, 7405-7413.

[29] Schilling S, Zeitschel U, Hoffmann T, Heiser U, Francke M, Kehlen A, Holzer M, Hutter-Paier B, Prokesch M, Windisch M, Jagla W, Schlenzig D, Lindner C, Rudolph T, Reuter G, Cynis H, Montag D, Demuth HU, Roßner S (2008) Glutaminyl cyclase inhibition attenuates pyroglutamate Abeta and Alzheimer's disease-like pathology. *Nature Med* **14**, 1106-1111.

[30] Schilling S, Appl T, Hoffmann T, Cynis H, Schulz K, Jagla W, Friedrich D, Wermann M, Buchholz M, Heiser U, von Hörsten S, Demuth HU (2008) Inhibition of glutaminyl cyclase prevents pGlu-Aβ formation after intracortical/hippocampal microinjection *in vivo*/in situ. *J Neurochem* **106**, 1225-1236.

[31] Fischer WH, Spiess J (1987) Identification of a mammalian glutaminyl cyclase converting glutaminyl into pyroglutamyl peptides. *Proc Natl Acad Sci U S A* **84**, 3628-3632.

[32] Busby WH, Quackenbush GE, Humm J, Youngblood WW, Kizer JS (1987) An enzyme(s) that converts glutaminyl-peptides into pyroglutamyl-peptides. *J Biol Chem* **262**, 8532-8536.

[33] Pohl T, Zimmer M, Mugele K, Spiess J (1991) Primary structure and functional expression of a glutaminyl cyclase. *Proc Natl Acad Sci U S A* **88**, 10059-10063.

[34] Böckers TM, Kreutz MR, Pohl T (1995) Glutaminyl-cyclase expression in the bovine/porcine hypothalamus and pituitary. *J Neuroendocrinol* **7**, 445-453.

[35] Morawski M, Hartlage-Rübsamen M, Jäger C, Waniek A, Schilling S, Schwab C, McGeer P, Arendt T, Demuth HU, Roßner S (2010) Distinct glutaminyl cyclase expression in Edinger-Westphal nucleus, locus coeruleus and nucleus basalis Meynert contributes to pGlu-Aβ pathology in Alzheimer's disease. *Acta Neuropathol* **120**, 195-207.

[36] Hartlage-Rübsamen M, Staffa K, Waniek A, Wermann M, Hoffmann T, Cynis H, Schilling S, Demuth HU, Roßner S (2009) Developmental expression and subcellular localization of glutaminyl cyclase in mouse brain. *Int J Dev Neurosci* **27**, 825-835.

[37] Hartlage-Rübsamen M, Morawski M, Waniek A, Jäger C, Zeitschel U, Koch B, Cynis H, Schilling S, Schliebs R, Demuth HU, Roßner S (2011) Glutaminyl cyclase contributes to the formation of focal and diffuse pyroglutamate (pGlu)-Aβ deposits in hippocampus via distinct cellular mechanisms. *Acta Neuropathol* **121**, 705-719.

[38] Alexandru A, Jagla W, Graubner S, Becker A, Bäuscher C, Kohlmann S, Sedlmeier R, Raber KA, Cynis H, Rönicke R, Reymann KG, Petrasch-Parwez E, Hartlage-Rübsamen M, Waniek A, Roßner S, Schilling S, Osmand AP, Demuth HU, von Hörsten S (2011) Selective hippocampal neurodegeneration in transgenic mice expressing small amounts of truncated Aβ is induced by pyroglutamate-Aβ formation. *J Neurosci* **31**, 12790-12801.

[39] Jawhar S, Wirths O, Schilling S, Graubner S, Demuth HU, Bayer TA (2011) Overexpression of glutaminyl cyclase, the enzyme responsible for pyroglutamate Abeta formation, induces behavioral deficits, and glutaminyl cyclase knockout rescues the behavioral phenotype in 5XFAD mice. *J Biol Chem* **286**, 4454-4460.

[40] Beach TG, Sue LI, Walker DG, Roher AE, Lue L, Vedders L, Connor DJ, Sabbagh MN, Rogers J (2008) The Sun Health Research Institute Brain Donation Program: Description and experience, 1987-2007. *Cell Tissue Bank* **9**, 229-245.

[41] Mai JK, Assheuer J, Paxinos G (2004) *Atlas of the human brain*. Academic Press, San Diego.

[42] Wirths O, Bethge T, Marcello A, Harmeier A, Jawhar S, Lucassen PJ, Multhaup G, Brody DL, Esparza T, Ingelsson M, Kalimo H, Lannfelt L, Bayer TA (2010) Pyroglutamate Abeta pathology in APP/PS1KI mice, sporadic and familial Alzheimer's disease cases. *J Neural Transm* **117**, 85-96.

[43] Konigsmark BW (1970) Methods for the counting of neurons. In *Contemporary Research Methods in Neuroanatomy*, Nauta WHJ, Ebbesson SOE, eds. Springer, Berlin, pp. 315-380.

[44] Andersen CL, Ledet-Jensen J, Ørntoft T (2004) Normalization of real-time quantitative RT-PCR data: A model based variance estimation approach to identify genes suited for normalization - applied to bladder- and colon-cancer data-sets. *Cancer Res* **64**, 5245-5250.

[45] Wirths O, Erck C, Martens H, Harmeier A, Geumann C, Jawhar S, Kumar S, Multhaup G, Walter J, Ingelsson M, Degerman-Gunnarsson M, Kalimo H, Huitinga I, Lannfelt L, Bayer TA (2010) Identification of low molecular weight pyroglutamate Abeta oligomers in Alzheimer disease: A novel tool for therapy and diagnosis. *J Biol Chem* **285**, 41517-41524.

[46] Frost JL, Liu B, Kleinschmidt M, Schilling S, Demuth HU, Lemere CA (2012) Passive immunization against pyroglutamate-3 amyloid-β reduces plaque burden in Alzheimer-like transgenic mice: A pilot study. *Neurodegener Dis* **10**, 265-270.

[47] Demattos RB, Lu J, Tang Y, Racke MM, Delong CA, Tzaferis JA, Hole JT, Forster BM, McDonnell PC, Liu F, Kinley RD, Jordan WH, Hutton ML (2012) A plaque-specific antibody clears existing β-amyloid plaques in Alzheimer's disease mice. *Neuron* **76**, 908-920.

[48] Weber F, Lues I, Meyer A, Hoffmann T, Pokorny R, Lopez L, Demuth HU, Glund K (2013) A phase 1 study assessing safety, pharmacokinetics and pharmacodynamics of PQ912, the first glutaminyl cyclase (QC) inhibitor to treat AD. *11th Conference on Alzheimer's disease and Parkinson's disease*. Florence, March 6-10, 2013; Abstract 1453.

[49] Saygin AP, Dick F, Wilson SM, Dronkers NF, Bates E (2003) Neural resources for processing language and environmental sounds: Evidence from aphasia. *Brain* **126**, 928-945.

[50] Jacobs J, Kahana MJ, Ekstrom AD, Mollison MV, Fried I (2010) A sense of direction in human entorhinal cortex. *Proc Natl Acad Sci U S A* **107**, 6487-6492.

[51] Suthana N, Haneef Z, Stern J, Mukamel R, Behnke E, Knowlton B, Fried I (2012) Memory enhancement and deep-brain stimulation of the entorhinal Area. *N Engl J Med* **366**, 501-510.

[52] Serrano-Pozo A, Frosch MP, Masliah E, Hyman BT (2011) Neuropathological alterations in Alzheimer's disease. *Cold Spring Harb Perspect Med* **1**, a006189.

[53] De Kimpe L, Bennis A, Zwart R, van Haastert ES, Hoozemans JJ, Scheper W (2012) Disturbed $Ca2^{+}$ homeostasis increases glutaminyl cyclase expression; connecting two early pathogenic events in Alzheimer's disease *in vitro*. *PLOS One* **7**, e44674.

[54] Valenti MT, Bolognin S, Zanatta C, Donatelli L, Innamorati G, Pampanin M, Zanusso G, Zatta P, Dalle Carbonare L (2013) Increased glutaminyl cyclase expression in peripheral blood of Alzheimer's disease patients. *J Alzheimers Dis* **34**, 263-271.

[55] Muresan Z, Muresan V (2008) Seeding neuritic plaques from the distance: A possible role for brainstem neurons in the development of Alzheimer's disease. *Neurodegener Dis* **5**, 250-253.

[56] Christensen DZ, Kraus SL, Flohr A, Cotel MC, Wirths O, Bayer TA (2008) Transient intraneuronal Aβ rather than extracellular plaque pathology correlates with neuron loss in the frontal cortex of APP/PS1 mice. *Acta Neuropathol* **116**, 647-655.